Accommodation of SiGe strain on a universally compliant porous silicon substrate

Isabelle Berbezier,[1,*] Jean-Noël Aqua,[2,†] Mansour Aouassa,[1] Luc Favre,[1] Stéphanie Escoubas,[1] Adrien Gouyé,[1] and Antoine Ronda[1]

[1]*Institut Matériaux Microélectronique Nanoscience de Provence, Aix-Marseille Université, UMR CNRS 6242, Avenue Escadrille Normandie Niemen - Case 142, 13997 Marseille, France*

[2]*Institut des Nanosciences de Paris, Sorbonne Universités, UPMC Univ Paris 06, UMR 7588, CNRS, F-75005, Paris, France*

(Received 1 April 2014; revised manuscript received 27 June 2014; published 21 July 2014)

The growth of heteroepitaxial planar fully strained SiGe layers with high Ge concentration and large thickness enables tailoring electronic properties for enhanced transport properties and photoemission. We give here the first experimental and theoretical proof that high temperature flashed porous silicon layers (HT-PSi) perfectly accommodate the stress of SiGe layers and provide compliant substrates with unprecedented capabilities for the fabrication of planar SiGe nanomembranes. We show that the stress driven morphological evolution leading to self-organized quantum dots commonly observed on nominal Si (001) is fully inhibited when growing SiGe on such a HT-PSi substrate. The elastic behavior of HT-PSi results from two specific features: It is ten times softer than Si and tensily strained. Theoretical analysis proves that the compliant behavior of HT-PSi is due to the strain effect, while on the contrary its elastic softness favors the development of 3D growth. The inhibition due to the tensile strain produces atomically flat layers free of misfit dislocation.

DOI: 10.1103/PhysRevB.90.035315 PACS number(s): 81.15.Hi, 68.35.Ct, 81.10.Aj, 46.70.Lk

I. INTRODUCTION

Advanced Si-based devices for electronic and optoelectronic applications commonly require SiGe heterostructures to optimize their performance. In the current planar Si-based technology, strain engineering is a critical strategy in tailoring the band-gap energy and the electronic properties for enhanced charge transport. Dislocation-free bidimensional heterostructures however cannot be grown with arbitrary thickness as the strain energy should not exceed that required to form either 3D islands or dislocations in the grown layer. To increase this critical thickness for the manipulation and integration into next-generation devices [1,2], it is of interest to grow the heterostructures on compliant substrates [3–8]. Si-based flexible nanomembranes (NMs) grown on such substrates have exceptional structural, mechanical, and electronic properties. These NMs on elastic soft substrates that can be stretched, compressed, and deformed are attractive for flexible opto- and nanoelectronics, photonics, and biological applications [9–16]. In addition to their mechanical properties, NMs offer a band-gap engineering ability controlled by the elastic-strain sharing with the compliant substrate [3–8].

Recently, porous Si (PSi) came back in front of the scene as a promising candidate in the highly competitive course for finding compliant substrates for the epitaxy of heterogeneous systems (III-V, SiGe ...) on Si. Its low cost fabrication and ease of integration in advanced CMOS technology provide significant benefits for Si-based optoelectronic integrated devices. Due to its porosity, PSi is a soft material with an elastic modulus almost ten times smaller than Si. It is therefore expected to accommodate the mismatch of heterogeneous layers and to serve as a mechanically stretchable pseudosubstrate. A two-step electrochemical formation process was recently developed in Refs. [17,18] which produced a PSi bilayer with an ultrathin atomically flat layer (where pores are stopped out) on top of a thick PSi highly porous layer. However, low temperature epitaxy of SiGe and Ge on such a bilayer produced rough epitaxial layers with extended defects [19–23].

We demonstrate here that high temperature flashed PSi bilayers (HT-PSi) behave as compliant substrates for the fabrication of relaxed planar SiGe NMs. The HT annealing produces a structural evolution where small pores transform into large pores while a tensile strain builds up [24]. Such a pseudosubstrate has then two striking characteristics: It is both very soft and tensily strained. When annealed at HT, the thick PSi undergoes a morphological and structural evolution with the transformation of small pores (∼10 nm) into large pores (∼500 nm) as already reported [24], while a tensile strain builds up in the thin top PSi layer free of pores. After deposition of SiGe/Si layers on HT-PSi, we show the inhibition of the morphological evolution commonly observed for SiGe on Si (reminiscent of the Asaro-Tiller-Grinfel'd, ATG, instability). Atomically flat layers free of misfit dislocation for thickness well above the critical thickness commonly measured on a Si substrate are produced. Theoretical analysis shows that the compliant behavior of HT-PSi is due to the tensile strain, while its softness conversely favors the development of the surface corrugation. This procedure paves the way to efficiently integrate heterogeneous systems on Si using HT-PSi either as a pseudosubstrate or as a NM.

II. EXPERIMENTAL

PSi bilayer structures are formed by electrochemical etching of a ⟨001⟩-oriented B-doped Si wafer dipped in hydrofluoric acid (HF) [25,26]. A thin top layer with low porosity is produced at higher electrocurrent to provide a good epitaxy of the next SiGe/Si layers [27]. In a second step, PSi layers are annealed under H atmosphere at high temperature T (1000 °C). Before introduction into the growth chamber, the HT-PSi/Si(001) substrates are first cleaned with a piranha solution [1:3 v/v H_2O_2 (30 wt. %):H_2SO_4(96 wt. %)] at 80 °C

*isabelle.berbezier@im2np.fr
†aqua@insp.jussieu.fr

 ©2014 American Physical Society

for 10 min, then rinsed in DI water and cleaned in HF:H_2O_2 (1:10) and rinsed again. After cleaning, they are immediately introduced into the UHV chamber to avoid contamination, where they are outgassed at 400 °C for 15 min. A Si buffer layer is deposited by MBE in UHV at 700 °C, before SiGe layers grown at 550 °C. The morphology and microstructure of the samples were investigated by atomic force microscopy (AFM) in air, transmission electron microscopy (TEM), and high resolution x-ray diffraction (HR-XRD). TEM cross-section observations were performed with a JEOL2010F at 200 keV. The crystalline structure was determined by HR-XRD with an X'Pert PRO MRD Diffractometer, using the $CuK_{\alpha 1}$ radiation ($\lambda = 1.54056$ Å). The MRD setup has a four circles goniometer with a sealed Cu x-ray tube and a 3 bounces Ge (220) analyzer used for HR measurements. Both $\Omega - 2\theta$ scans and reciprocal space mappings are performed, respectively, for the Si (004) and (224) reflexions. The (004) XRD pattern allows the determination of the vertical lattice parameter. The (224) reciprocal space mapping allows the determination of the strain relaxation and Ge composition. Both symmetric and asymmetric scans were also performed. The sample is a (001) oriented Si wafer; the (004) Bragg peak was mapped with the [004] direction normal to the plane of the wafer. [224] is a direction within the plane of the film. Position in q_z correlates to the d spacing of the peak; position in q_x correlates to tilt of planes. Map of the symmetric Bragg peak is used to separate tilts and strain, and map of the asymmetric peak is used to separate composition and strain.

III. RESULTS AND DISCUSSION

A. Evolution and strain

SiGe layers are deposited on a bilayer HT-PSi/Si(001) substrate which consists of a thick porous layer with large pores (produced during the high temperature annealing) and a thin flat layer almost free of pores at the top surface. During HT annealing, which stabilizes the PSi chemical nature, a morphological transformation is observed: The small and dense pores coalesce into large pores ~500 nm in diameter [see TEM cross sections of Fig. 1(a)]. An ultrathin Si buffer layer is then deposited by molecular beam epitaxy in ultrahigh vacuum (UHV) at 700 °C to provide a perfect cleanliness and reproducibility of the surface free of contaminant, before the growth of SiGe layers at 550 °C, see Fig. 1. The epitaxy of the Si buffer layer on top of the substrate is facilitated by the atomically flat top surface of the HT-PSi. It produces a nice Si buffer layer free of defect and fully coherent with the substrate, see Fig. 1. The XRD $\Omega - 2\theta$ scan of the Si/HT-PSi/Si(001) system, Fig. 1(b), shows different peaks representative of the different lattice parameters in the growth direction $a_\perp$. The double peak is ascribed to the Si(001) substrate and to the HT-PSi. This double peak has already been observed in a recent paper [20]. The small tensile strain observed in PSi was explained by the desorption of −OH species during annealing [28]. An additional broad peak not observed in the previous work (single HT-PSi layer) is now visible on the right side (right arrow). Since it was not observed previously, it may be ascribed to the top thin PSi layer free of pore and performed in different electrochemical conditions. Its angular position demonstrates a tensily strained layer. We measure $a_\perp^{\mathrm{PSi}} = 5.405$ Å. In the presence of an in-plane strain $\eta = (a_\parallel^{\mathrm{PSi}} - a^{\mathrm{PSi}})/a^{\mathrm{PSi}}$ with the in-plane lattice parameter $a_\parallel$, the Poisson dilatation leads to a tetragonal distortion $a_\perp^{\mathrm{PSi}} = a^{\mathrm{PSi}}[1 - 2\nu\eta/(1-\nu)]$ with the Poisson ratio ν. With our measure, we find $a_\parallel^{\mathrm{PSi}} = 5.465$ Å so that $\eta = 0.63\%$ with $a^{\mathrm{PSi}} = a^{\mathrm{Si}}$. This tensile strain is induced by the HT annealing which causes the swelling of the lattice structure. These data are confirmed by the (224) map, see inset in Fig. 1.

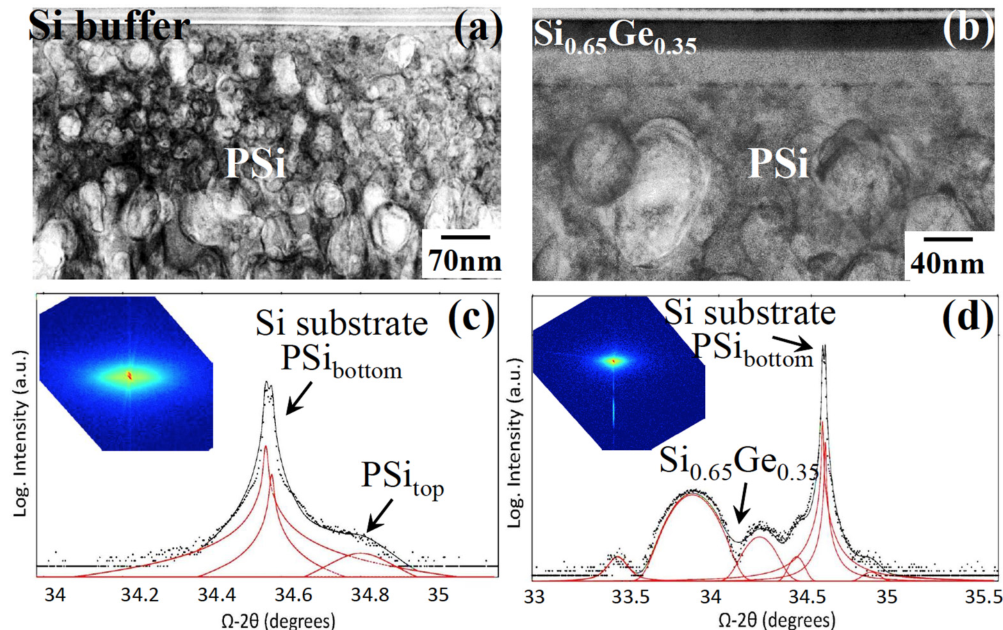

FIG. 1. (Color online) (a) and (c) TEM cross-section images and (b) and (d) corresponding XRD $\Omega - 2\theta$ scans for (a) and (b) a Si buffer layer/HT-PSi and (c) and (d) SiGe film ($x = 0.35$, $h = 27$ nm)/Si buffer layer/HT-PSi. HT-PSi exhibits in both cases large pores underneath and smaller pores in the very top layer. The insets give the corresponding (224) reciprocal map in the two situations.

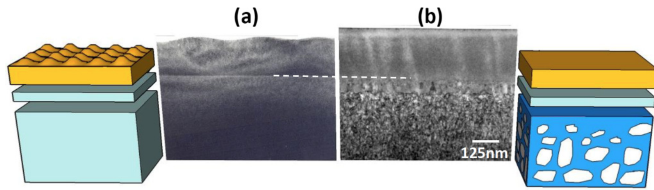

FIG. 2. (Color online) Comparison of the two systems investigated: (a) SiGe/Si(001) bulk substrate and (b) SiGe/HT-PSi/Si(001) bulk substrate. Schematic cross-section representations of the layers and TEM cross-section images of $Si_{1-x}Ge_x$ with $x = 0.15$ deposited on (left) Si(001) with $h_{SiGe} = 150$ nm and (right) HT-PSi with $h_{SiGe} = 250$ nm.

On top of this Si/HT-PSi bilayer, we deposited $Si_{1-x}Ge_x$ layers with different compositions in between $x = 0.15$ and 0.35 and with thicknesses lower than the critical thickness for the nucleation of misfit dislocation [29]. We compare the morphological evolution of SiGe on Si(001) on the one hand and on the PSi stressor on the other. For these compositions and thicknesses, the morphological ATG instability does indeed occur on Si(001) [29,30]. Conversely, in the same experimental conditions, the instability is inhibited on HT-PSi. This behavior is typically exemplified for $x = 0.35$ and for a thickness $h = 27$ nm that usually lead to the ATG instability on Si(001), see Figs. 2 and 3. In these conditions, we find that the SiGe film deposited on the HT-PSi stressor is perfectly planar and free of extended defect as seen by TEM cross section, Fig. 1(c). The XRD map along [224] and $\Omega - 2\theta$ spectra along [004] show that the epitaxial SiGe film is fully coherent with the HT-PSi stressor, Fig. 1(d). On the latter, one can see from right to left the PSi and Si(001) peaks, and the peaks assessed to the SiGe layer and its interferences due to reflexions with interfaces. The well-developed interferences attest to the very good crystalline quality of the SiGe layer. The angular position of the SiGe peak gives $a_\perp^{SiGe} = 5.536$ Å while the angular position of the HT-PSi peak is unchanged after deposition of SiGe ($a_\perp^{PSi} = 5.405$ Å so that $a_\parallel^{PSi} = 5.465$ Å). Moreover, the (224) map, plotted in the coordinates q_x and q_z perpendicular and along the growth direction, reveals a perfect alignment of the SiGe and HT-PSi peaks and the coherence of the system. One may thence consider $a_\parallel^{SiGe} = a_\parallel^{PSi}$ so that $a_\perp^{SiGe}$ is consistent with the mean film composition $x = 0.35$ using the documented values of the SiGe lattice parameter [31].

A similar behavior is obtained for larger SiGe thickness/lower Ge concentration. As an example, for $x = 0.15$ we find again that the morphological instability is inhibited on the HT-PSi stressor for thicknesses up to 250 nm while, the SiGe growth on Si(001) produces a corrugated film even for $h = 150$ nm, see Figs. 2 and 3. The typical cross-section TEM images of the SiGe layer evidence an atomic flatness of the surface and the absence of misfit dislocation when using the HT-PSi substrate, while the typical morphology of the ATG instability is observed for the epitaxy on Si(001). This difference is attested by the different root mean square roughness of the as-grown layers [respectively, 0.13 and 3.2 nm on the HT-PSi stressor and Si(001)]. From this experimental part, we conclude that the HT-PSi stressor substrate plays a major role on the morphological evolution of the SiGe epilayer. This finding could result from different effects: (i) the tensile state of the stressor reported above; (ii) the well-known softness of the PSi layer [18]. We thence focus in the following on the competition between these two effects [32].

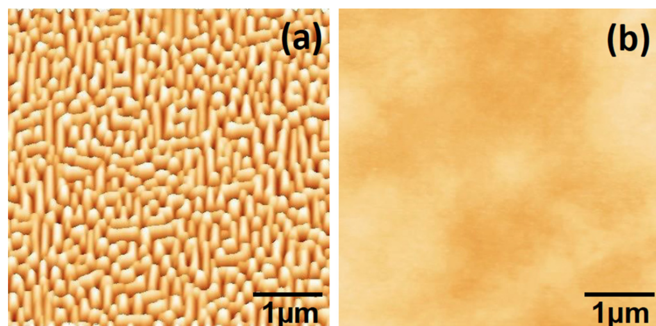

FIG. 3. (Color online) Atomic force microscopy images of the SiGe top surfaces corresponding to the images displayed in Fig. 2: (a) SiGe/Si(001) bulk substrate and (b) SiGe/HT-PSi/Si(001) bulk substrate on Si(001). RMS roughness is 3.2 nm and 0.13 nm for (a) and (b), respectively. The height scale is identical for the two images (between 0 and the maximum height 15 nm).

B. Morphological evolution

We reconsider the theoretical description of the morphological evolution of strained films resulting from elastic relaxation enforced by surface diffusion [33,34]. The geometry under scrutiny is a SiGe film on top of a Si buffer layer in epitaxy on a porous substrate, Fig. 2. Strain arises as the film and buffer layer have a lattice mismatch $m = (a^{SiGe} - a^{Si})/a^{Si}$ while their interface is coherent. As a first approximation, we consider that SiGe and Si have equal Young modulus Y and Poisson ratio ν. Conversely, the porous medium is described as a continuous but softer system with a different Young modulus $Y_{PSi} = s\,Y$ which evolves with the porosity ϕ as $s = (1-\phi)^2$, see Refs. [18,35,36]. The observation of the coherence of the film/buffer and PSi/Si interfaces enforces the continuity at these interfaces of both the displacements and forces, while the upper film surface at $z = h(\boldsymbol{r},t)$ with $\boldsymbol{r} = (x,y)$ is free of stress. The $z = 0$ reference plane corresponds to the lower Si interface with PSi. Finally, we account for an in-plane tensile strain η in PSi by imposing the displacement $\boldsymbol{u}^\eta = \eta\{x,y,-2\nu z/(1-\nu)\}$ deeply in PSi (with the Poisson distortion in the z-component). On the instability time scale, mechanical equilibrium is promptly realized and one may solve the elasticity equations at equilibrium in a quasistatic approach.

The strain relaxation leading to the ATG instability depends on the level of stress in the initial flat film when $h(\boldsymbol{r}) = \bar{h} = e + h$, with h and e, the SiGe film and Si buffer layer thicknesses. In this geometry, the forces, stress tensor, and displacement gradients are independent of (x,y), and we find that the displacement vector at mechanical equilibrium is

$$\boldsymbol{u}_0 = \boldsymbol{u}^\eta + m^\alpha \frac{1+\nu}{1-\nu}(z-e)\,\{0,0,1\}\,, \tag{1}$$

where $m^f = m$ in the film and $m^{b/p} = 0$ in the buffer and PSi (b/p). This displacement field is associated with the

energy density $\bar{\mathcal{E}}_0 = \mathcal{E}_0(1-\eta/m)^2$ with $\mathcal{E}_0 = Ym^2/(1-\nu)$. The energy stored in the flat film is commonly relaxed either via a morphological evolution or via dislocations. It is significantly dependent here on the substrate strain level through the $(1-\eta/m)^2$ term.

The energy stored in $\boldsymbol{u}_0$ may be relieved when a morphological modulation of the surface leads to a global energy gain. To estimate the elastic driving force, one should compute the strain relaxation induced by a modulation $h(\boldsymbol{r},t) = \bar{h} + h_1(\boldsymbol{r},t)$ where h_1 displays small slopes. For such a surface, we find a solution as $\boldsymbol{u} = \boldsymbol{u}_0 + \boldsymbol{u}_1$ where $\boldsymbol{u}_1$ is computed thanks to a Fourier transform ($\mathcal{F}$) over $\boldsymbol{r}$ with the wave vector $\boldsymbol{k}$. The associated elastic energy density reads at first order

$$\mathcal{E} = \bar{\mathcal{E}}_0 - 2(1+\nu)\bar{\mathcal{E}}_0\,\mathcal{F}^{-1}[A_k\,k\,h_1(\boldsymbol{k})], \tag{2}$$

where

$$A_k = \frac{a\,e^{2k\bar{h}} - b\,e^{-2k\bar{h}} - 4\,k\bar{h}}{a\,e^{2k\bar{h}} + b\,e^{-2k\bar{h}} - (1+ab) - 4k^2\bar{h}^2}, \tag{3}$$

with $a = (1+3s-4s\nu)/(1-s)$ and $b = (1-s)(3-4\nu)/(3+s-4\nu)$. Note that the $\bar{h}$ dependance which arises here is due to finite size effects in the Si layer. Combined with capillary effects, the elastic strain leads to a surface diffusion given by the diffusion equation

$$\frac{\partial h}{\partial t} = D\boldsymbol{\Delta}\mu, \tag{4}$$

with the diffusion constant D and the chemical potential $\mu = \mathcal{E} - \gamma\,\boldsymbol{\Delta}h$ which accounts both for the elastic energy $\mathcal{E}$ and the surface energy γ [37]. With our solution, we find that a harmonic corrugation h_1 evolves in Fourier space as $h_1(\boldsymbol{k},t)e^{\sigma t}e^{i\boldsymbol{k}\cdot\boldsymbol{r}}$ with the growth rate σ of the corrugation,

$$\sigma = A_k\,(1-\eta/m)^2\,k^3 - k^4, \tag{5}$$

in units of the space and time scales

$$l_0 = \gamma/[2(1+\nu)\mathcal{E}_0] \quad \text{and} \quad t_0 = l_0^4/D\gamma. \tag{6}$$

Note that l_0 and t_0 which dictate the wave vector with maximum growth rate are significantly sensitive to the misfit and evolve as $1/m^2$ and $1/m^8$, respectively (for $x = 0.3$, one finds $l_0 = 13$ nm and $t_0 = 270$ s, see. e.g., Ref. [30]). For a corrugation with a given k, a positive σ signals the growth of such a corrugation, while a negative value corresponds to its damping. In the limit of equal elastic constants in the entire system ($s = 1$) and in the absence of any prestrain $\eta = 0$, one retrieves the ATG spectrum [33,34] $\sigma_{\text{ATG}}(k) = k^3 - k^4$. In the general case however, the expansion of A_k at low k leads to $\sigma \approx k^3(1-\eta/m)^2/s - \alpha k^4$ with a coefficient α of order unity.

These results first evidence the counterintuitive effect that the softness of the porous medium leads to the enhancement of the instability. It is manifest in the $1/s$ amplitude of the k^3 term in the small-k expansion of σ, and confirms the tendency found in Ref. [37]. It may be rationalized by the fact that the elastic relaxation on the surface is associated with a smaller but nonzero strain in the substrate, which is reduced by the softness of the substrate. Hence, the inhibition of the instability on HT-PSi may not be explained by the softness of the porous medium in epitaxy with a bulk substrate. It is clearly visible in Fig. 4 where σ for a soft unstrained pseudosubstrate (dashed red line) is always greater than its corresponding value for a Si(001) (solid blue line). We note that indeed, on a PSi substrate before HT annealing (not tensily strained), we did observe a strain relaxation larger than on Si(001) [20].

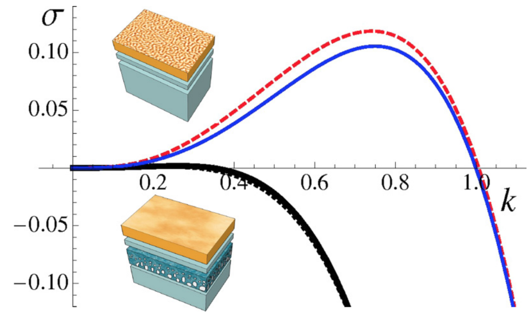

FIG. 4. (Color online) Growth rate σ as a function of the wavevector k of the morphological instability of a strained SiGe film on top of a Si buffer deposited on: (thick solid black line) a tensile and soft porous medium (typically HT-PSi); (thick dotted black line) a tensile medium with equal stiffness; (dashed red line) a soft medium without prestrain; (solid blue line) a medium without prestrain and with equal stiffness [nominal bulk Si(001) substrate] corresponding to σ_{ATG}. The parameters correspond to the experiments described in the text. The figure is given in dimensionless units corresponding to the instability length and time scales l_0 and t_0 given in Eq. (6).

On the other hand, the $(1-\eta/m)^2$ amplitude in Eq. (5) is ascribed to the tensile state of HT-PSi which reduces the effective in-plane strain experienced by SiGe. It leads to a dramatic reduction of σ when the tensile strain measured in experiments is accounted for on Si(001), see the thick dotted black line in Fig. 4. The growth rate resulting from both the substrate softness and tensile strain is then plotted with the experimental values described above, $x = 0.35$, $h = 27$ nm, $e = 20$ nm, $\phi = 50\%$, and $\eta = 0.63\%$. The important result of this analysis is that the instability growth rate remains mainly negative when both the softness and tensile state are included, see thick solid black line in Fig. 4. Consequently, the perturbation analysis predicts in these conditions that the film remains flat, similarly to the experimental finding on the HT-PSi stressor. The tensile strain overcompensates in this case the effect of the softness. The same result is found for the parameters of the $x = 0.15$ film even for the thickness $h = 250$ nm displayed in Fig. 2. On the contrary, the typical $k^3 - k^4$ ATG growth rate which exhibits a full range of unstable wave vectors with $\sigma > 0$, Fig. 4, is relevant for a SiGe film on a Si substrate ($\eta = 0$, $s = 1$) where the growing instability eventually leads to self-organized quantum dots [30], see Fig. 2.

IV. CONCLUSION

In summary, we managed to grow thick, planar, and dislocation-free SiGe nanomembranes on top of a high temperature flashed PSi bilayer substrate. Contrary to equivalent layers grown on bulk Si(001), the SiGe layers do not exhibit the usual morphological instability related to strain relaxation, even for a thickness well above the critical thicknesses of this effect. The striking strain accommodation provided by HT-PSi is explained theoretically by computing the growth

rate of a corrugation in the presence of a (i) tensily strained and (ii) soft substrate. We show that, counterintuitively, the latter enhances the morphological evolution while the former inhibits its onset. Given the strain level that was measured by XRD, we find that the competition between these two effects is dominated by the tensile strain and leads to the kinetic inhibition of the instability. The high-temperature annealing of PSi which generates this tensile strain produces a unique material highly suitable as a substrate for the heterogeneous integration of various systems on Si. The low-cost process developed here takes also benefits from the chemical stability and reproducibility of HT-PSi, which is in addition fully compatible with the CMOS technology. These results open the way for developing new metamaterials through heterogeneous epitaxy on free-standing SiGe/HT-PSi nanomembranes lift off from the Si substrate.

[1] P. M. Mooney, G. M. Cohen, J. O. Chu, and C. E. Murray, Appl. Phys. Lett. **84**, 1093 (2004).
[2] S. A. Scott and M. G. Lagally, J. Phys. D: Appl. Phys. **40**, R75 (2007).
[3] M. Huang, C. S. Ritz, B. Novakovic, D. Yu, Y. Zhang, F. Flack, D. E. Savage, P. G. Evans, I. Knezevic, F. Liu, and M. G. Lagally, ACS Nano **3**, 721 (2009).
[4] A. Malachias, Y. Mei, R. K. Annabattula, C. Deneke, P. R. Onck, and O. G. Schmidt, ACS Nano **2**, 1715 (2008).
[5] D.-Y. Khang, H. Jiang, Y. Huang, and J. A. Rogers, Science **311**, 208 (2006).
[6] L. Zhang, E. Ruh, D. Grützmacher, L. Dong, D. J. Bell, B. J. Nelson, and C. Schönenberger, Nano Lett. **6**, 1311 (2006).
[7] M. M. Roberts, L. J. Klein, D. E. Savage, K. A. Slinker, M. Friesen, G. Celler, M. A. Eriksson, and M. G. Lagally, Nat. Mater. **5**, 388 (2006).
[8] M. Huang, C. Boone, M. Roberts, D. E. Savage, M. G. Lagally, N. Shaji, H. Qin, R. Blick, J. A. Nairn, and F. Liu, Adv. Mater. **17**, 2860 (2005).
[9] M. Ying, A. P. Bonifas, N. Lu, Y. Su, R. Li, H. Cheng, A. Ameen, Y. Huang, and J. A. Rogers, Nanotechnology **23**, 344004 (2012).
[10] X. Xu, H. Subbaraman, A. Hosseini, C.-Y. Lin, D. Kwong, and R. T. Chen, Opt. Lett. **37**, 1020 (2012).
[11] J. Viventi, D.-H. Kim, L. Vigeland, E. S. Frechette, J. A. Blanco, Y.-S. Kim, A. E. Avrin, V. R. Tiruvadi, S.-W. Hwang, A. C. Vanleer, D. F. Wulsin, K. Davis, C. E. Gelber, L. Palmer, J. Van der Spiegel, J. Wu, J. Xiao, Y. Huang, D. Contreras, J. A. Rogers, and B. Litt, Nat. Neurosci. **14**, 1599 (2011).
[12] D.-H. Kim and J. A. Rogers, Adv. Mater. **20**, 4887 (2008).
[13] I. Tiginyanu, V. Popa, and M. A. Stevens-Kalceff, in *Proceedings of SPIE, Vol. 8068, Bioelectronics, Biomedical, and Bioinspired Systems V: and Nanotechnology V*, edited by A. B. Rodríguez Vázquez *et al.* (SPIE, Bellingham, WA, 2011), p. 806814.
[14] K. D. Hobart, F. J. Kub, M. Fatemi, M. E. Twigg, P. E. Thompson, T. S. Kuan, and C. K. Inoki, J. Elec. Mat. **29**, 897 (2000).
[15] G. M. Cohen, P. M. Mooney, V. K. Paruchuri, and H. J. Hovel, Appl. Phys. Lett. **86**, 251902 (2005).
[16] A. Ghaffari, A. Hosseini, X. Xu, D. Kwong, H. Subbaraman, and R. T. Chen, Opt. Express **18**, 20086 (2010).
[17] M. M. Wilkins, A. Boucherif, R. Beal, J. E. Haysom, J. F. Wheeldon, V. Aimez, R. Arès, T. J. Hall, and K. Hinzer, IEEE J. Photovolt. **3**, 1125 (2013).
[18] N. P. Blanchard, A. Boucherif, Ph. Regreny, A. Danescu, H. Magoariec, J. Penuelas, V. Lysenko, J.-M. Bluet, O. Marty, G. Guillot, and G. Grenet, *Engineering Materials* (Springer, Berlin, Heidelberg, 2011), p. 47.
[19] W. H. Thompson, Z. Yamani, H. M. Nayfeh, M.-A. Hasan, J. E. Greene, and M. H. Nayfeh, MRS Proceedings **452**, 255 (1996).
[20] M. Aouassa, S. Escoubas, A. Ronda, L. Favre, S. Gouder, R. Mahamdi, E. Arbaoui, A. Halimaoui, and I. Berbezier, Appl. Phys. Lett. **101**, 233105 (2012).
[21] S. Gardelis, A. G. Nassiopoulou, M. Mahdouani, R. Bourguiga, and S. Jaziri, Phys. E (Amsterdam, Neth.) **41**, 986 (2009).
[22] J. Salonen, E. Mäkilä, J. Riikonen, T. Heikkilä, and V. P. Lehto, Phys. Stat. Sol. (a) **206**, 1313 (2009).
[23] Y. H. Ogata, N. Yoshimi, R. Yasuda, T. Tsuboi, T. Sakka, and A. Otsuki, J. Appl. Phys. **90**, 6487 (2001).
[24] S. Gouder, R. Mahamdi, M. Aouassa, S. Escoubas, L. Favre, A. Ronda, and I. Berbezier, Thin Solid Films **550**, 233 (2014).
[25] G. Bomchil, A. Halimaoui, and R. Herino, Microelec. Eng. **8**, 293 (1988).
[26] G. Bomchil, A. Halimaoui, and R. Herino, Appl. Surf. Sci. **41**, 604 (1989).
[27] L. Vescan, G. Bomchil, A. Halimaoui, A. Perio, and R. Herino, Mat. Lett. **7**, 94 (1988).
[28] O. Bisi, S. Ossicini, and L. Pavesi, Surf. Sci. Rep. **38**, 1 (2000).
[29] J.-N. Aqua, I. Berbezier, L. Favre, T. Frisch, and A. Ronda, Phys. Rep. **522**, 59 (2013).
[30] J.-N. Aqua, A. Gouyé, A. Ronda, T. Frisch, and I. Berbezier, Phys. Rev. Lett. **110**, 096101 (2013).
[31] J. P. Dismukes, L. Ekstrom, and R. J. Paff, J. Phys. Chem. **68**, 3021 (1964).
[32] J.-N. Aqua, A. Gouyé, T. Auphan, T. Frisch, A. Ronda, and I. Berbezier, Appl. Phys. Lett. **98**, 161909 (2011).
[33] R. J. Asaro and W. A. Tiller, Metall. Trans. **3**, 1789 (1972).
[34] M. A. Grinfeld, Sov. Phys. Dokl. **31**, 831 (1986).
[35] J.-N. Aqua, T. Frisch, and A. Verga, Phys. Rev. B **76**, 165319 (2007).
[36] J.-N. Aqua, T. Frisch, and A. Verga, Phys. Rev. E **81**, 021605 (2010).
[37] B. J. Spencer, P. W. Voorhees, and S. H. Davis, Phys. Rev. Lett. **67**, 3696 (1991).